Spectral splitting and quantum path study of high-harmonic generation from a semi-infinite gas cell

2012 J. Phys. B: At. Mol. Opt. Phys. 45 074013

(http://iopscience.iop.org/0953-4075/45/7/074013)

J. Phys. B: At. Mol. Opt. Phys. **45** (2012) 074013 (8pp) doi:10.1088/0953-4075/45/7/074013

Spectral splitting and quantum path study of high-harmonic generation from a semi-infinite gas cell

W Cao, G Laurent, Cheng Jin, H Li, Z Wang, C D Lin, I Ben-Itzhak and C L Cocke

J R Macdonald Laboratory, Kansas State University, Manhattan, KS 66506, USA

E-mail: caowei1688@gmail.com

Received 4 October 2011, in final form 24 November 2011
Published 16 March 2012
Online at stacks.iop.org/JPhysB/45/074013

Abstract

We have investigated the spectral splitting of high harmonics generated in a semi-infinite gas cell. By performing an EUV–IR cross-correlation experiment, we are able to use the phase behaviour of the different sub-peaks of each harmonic to identify them with different electronic trajectories. Both microscopic and macroscopic analyses of the spectra effects are made. The identification of a particular trajectory with a particular component of the splitting on the basis of a single-atom model is found to be incorrect, while the full macroscopic treatment is in agreement with the experiment.

(Some figures may appear in colour only in the online journal)

1. Introduction

When atoms and molecules are exposed to strong electromagnetic fields, electrons can be stripped partially. In a time scale of the order of several atomic units (∼24 as), the resulting electron wave packet can involve both continuum and bound electronic states. The coupling between the bound and free electrons in the presence of the strong field leads to numerous interesting physical phenomena such as multi-photon ionization, tunnelling ionization, sequential/non-sequential double ionization and high-harmonic generation (HHG). Among these, HHG has been studied extensively in the last decade due to its potential applications in attosecond science [1–3] and as a coherent EUV source [4, 5]. HHG has also been applied to molecular orbital tomography [6] and time-resolved studies of molecules [7].

The three-step model [8] conceptually describes the process of HHG from a classical point of view. Two well-known major quantum paths of the returning electron (short and long trajectories) have been identified in this intuitive classical picture. Many topics associated with these quantum paths have been raised since then. In order to control and optimize the attosecond pulse train (APT), it has often been expedient to eliminate, through quantum path control, one or the other of these paths. Macroscopically, this can be realized either by playing with the optical geometry [9, 10] or by using a spatial filter [11]. Microscopically, a bichromatic electric field has been used as an efficient tool to enhance one or the other path by controlling the timing of the ionization step [12–14]. On the other hand, if the study of the underlying formation of the HHG is the intent, information can be gained from the quantum path interference between the two components. In this case, the participation of both paths with similar amplitudes is preferable to obtain optimal contrast in the interference pattern [15, 16].

One phenomenon which can result from the participation of both paths is the spectral splitting of each harmonic into two components. This phenomenon has been studied and observed by several groups [17–21]. Wang *et al* [17] reported that intensities well above the saturation value for argon produced a spectral splitting and proposed that the cause was a propagation effect resulting in a splitting of the harmonic pulse envelope into two components accompanied by a related spectral splitting. Zhong *et al* [18] also reported the HHG splitting in the over-saturated intensity region. They did a similar 1D propagation of HHG and found that the plasma's induced distortion of the fundamental field played a key role in the splitting of HHG. Brunetti *et al* [19] reported the

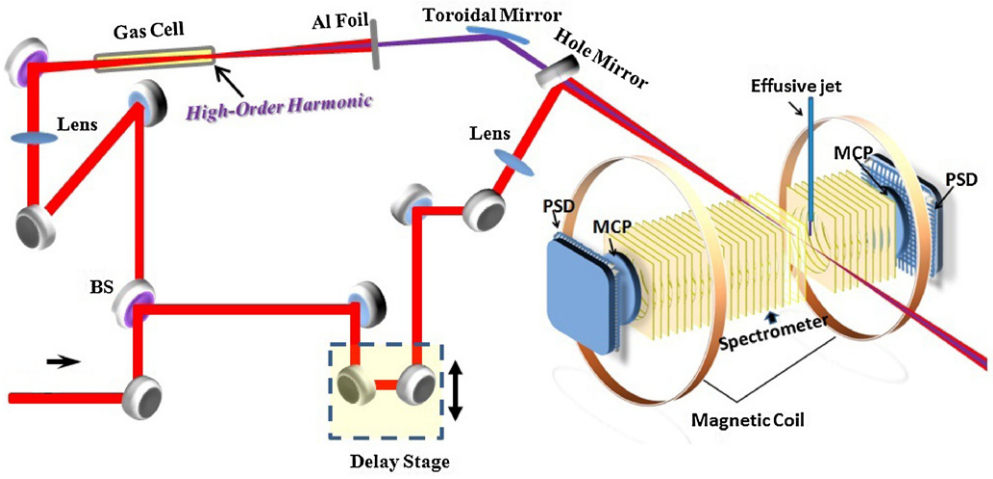

Figure 1. The schematic of the experimental setup.

substructure in each harmonic and attributed the splitting to properties of the single-atom response. Xu *et al* [20] observed a splitting of HHG generated at 1240 nm and attributed the structure to interference between short and long trajectories. He *et al* [21] observed the double and even triple peak structure in argon HHG, and interpreted this in terms of quantum path interference between short and long trajectories. They found that propagation effects enhanced the phase matching for the long trajectory making it of an intensity competitive with the short trajectory.

All previous measurements on the spectral splitting have been limited to intensity profiles. In order to gain deeper insight into the HHG process, it is necessary to know the phase as well as the intensity of each harmonic. In this paper, we provide such phase measurements. We do this by performing an EUV–IR cross-correlation experiment (RABBITT [22–25]). When the HHG are synchronized with a weak fundamental laser field and both fields interact with atoms, photoelectrons are produced via a two-photon process with energies sitting between those produced by adjacent harmonic photoelectrons (we will call these sideband photoelectrons hereafter). As can be explained from second-order perturbation theory, the sideband amplitude oscillates with EUV–IR delay with a periodicity of one half cycle of the fundamental field. The phase of the sideband oscillation corresponds to the first derivative of the phase of the HHG with respect to harmonic number, and thus a measurement of this oscillation yields experimental information on the phase of the HHG. In this paper, we use this phase information in addition to the spectra to investigate the physical processes which lead to the spectral splitting.

2. Experimental setup

The schematic of the experimental setup is shown in figure 1. The 2 mJ 50 fs laser beam generated from a commercial Ti:sapphire laser system is divided into two halves by a beam-splitter (BS). Part of the beam is focused by a 50 cm spherical lens into a gas cell filled with argon gas for HHG. A diaphragm is placed before the lens to control and adjust the laser beam diameter. We use a semi-infinite gas cell which is similar to that used in [25]. The cell is 30 cm long sealed with an AR-coated entrance window at one end and an exchangeable metal plate at the other end. The semi-infinite gas cell has the advantage over a gas jet that it has a higher conversion efficiency because of the increased focusing volume [26]. Another advantage is the improved stability of the spectrum due to the relatively stable gas flow in the interaction region. Since many parameters (gas pressure, focus position, beam diameter, etc) will affect the spectrum of HHG in order to systematically investigate the dependence of the spectrum on the location of the interaction region within the gas, we fix the gas pressure (30 Torr) and diaphragm at a position (0.8 cm in diameter) where reasonable flux is obtained, and then scan the focal position of the driving field along the direction of propagation of the laser. The peak intensity of the driving field is estimated to be no more than 6×10^{14} W cm^{-2} in vacuum. A 200 nm aluminum foil is used to block the IR beam after the gas cell. One meter downstream of the harmonic generation region, a toroidal reflector is applied at a grazing angle of 7° to deliver the EUV into the interaction region. The other part of the beam after the BS is passed through a piezoelectric transducer delay stage and recombines with the EUV beam via a hole mirror. The 2 mm hole is equivalent to a spatial filter for the EUV beam, limiting the angular spread of the HHG observed.

After recombination, the IR and EUV beams propagate collinearly and are focused onto the gas target located in the detection system. Photoelectrons from the interaction of the beams with the gas jet are detected by a position- and time-sensitive channel-plate detector, from which their energies are determined. Further details on the cold target recoil ion momentum spectroscopy (COLTRIMS) spectrometer are described in [27, 28]. For the present experiment, the COLTRIMS spectrometer was operated field free and only electrons were detected.

3. Experimental results

Figure 2 shows the photoelectron spectra of argon generated from HHG without IR. The photon energies of the EUV can

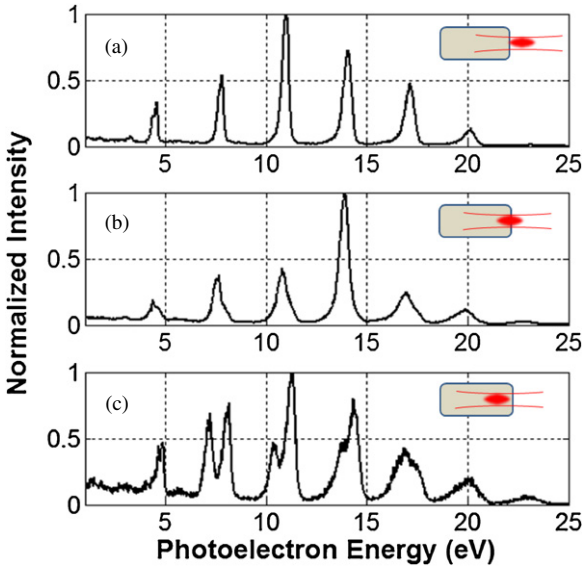

Figure 2. Experimental argon photoelectron spectra of harmonics generated with three different focusing geometries. The focal point is located (a) 3 mm after, (b) at and (c) 6.3 mm before the exit of the gas cell. The red dots indicate the focusing volume of the laser.

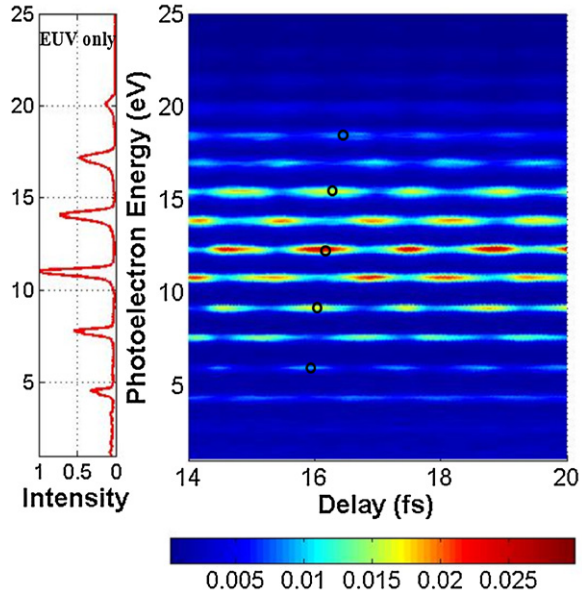

Figure 3. Left panel: the argon photoelectron spectrum when only the EUV is present. Right panel: the argon photoelectron spectrum versus EUV–IR delay. For specific delay, the spectrum has been normalized to the laser shots. The HHG were generated under the condition of figure 2(a) (focus beyond gas cell, case I) except that the IR was added. The black open circles indicate the positions of the maxima in the sideband oscillations.

be obtained from the photoelectron energy by adding the first ionization potential of argon (15.76 eV) to the photoelectron energy. When the driving pulse is focused outside the gas cell (3 mm beyond the exit aperture, case I), clean and sharp HHG peaks are observed indicating that a single quantum path (short trajectory) has been selected [29]. When we move the focal point to coincide with the exit aperture of the gas cell (case II), the HHG peaks start to get broader. When the focal point is located before the cell exit (6.3 mm before the exit aperture, case III), a clear double-peak structure is observed for each harmonic. This observation is consistent with the results from [17] and [19], which means that this could be a general and universal phenomenon in harmonics.

When the IR is present, the photoelectron spectrum develops sidebands which oscillate in intensity as the delay between the IR and EUV is varied. The phase of this oscillation can be used to extract the relative phases of the harmonics which are adjacent to each sideband using the well-established RABBITT technique [22–25]. Figure 3 shows a RABBITT scan corresponding to case I with the focus beyond the gas cell. No splitting of the HHG is observed for this case, and the oscillation maxima of the sidebands lie on a nearly straight line with a small positive slope. As discussed in [24], this slope is the characteristic of the HHG chirp expected for short trajectories.

Figure 4 shows the corresponding RABBITT scan for case III, for which strong spectral splitting is observed. The spectrum is somewhat busy due to the presence of sidebands from both the blue (higher energy) and red (lower energy) sub-peaks of each split harmonic. The expected locations of the sidebands from each component are indicated in the figure. It is immediately clear that the oscillation maxima of the blue and red sidebands line up along quite different straight lines, indicating that the chirps of the two components are quite different in both sign and size. The blue component has a small

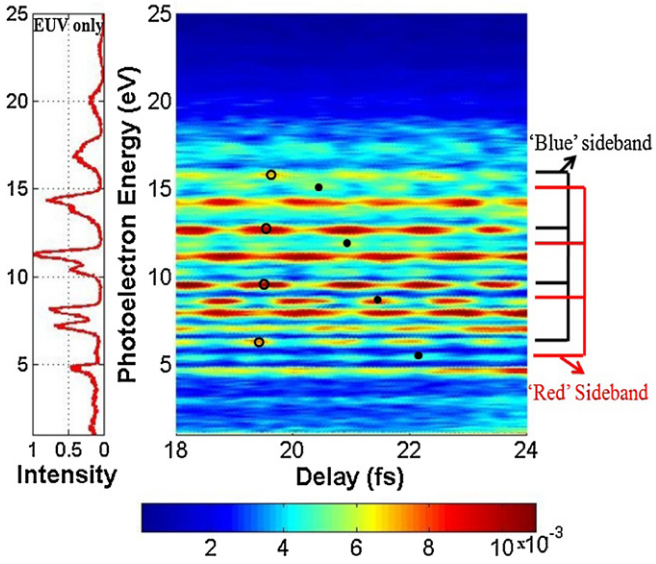

Figure 4. The same as figure 3 except that the harmonics are generated under the conditions of figure 2(c) (focus inside the gas cell, case III). The black open circles and black dots indicate the maxima of the oscillations of the two sideband groups located between each pair of HHG.

positive slope similar to that seen for case I and consistent with that expected for short trajectories. The red component has a large negative chirp, of the sign expected for long trajectories.

In the usual RABBITT analysis, the IR pulse is restricted at low intensities so that second-order perturbation theory can be used to analyse the spectrum. In figures 3 and 4, the amplitude of the sideband peaks is comparable to that of the main peaks and one might question whether the probe

intensity that we used is too high for a valid RABBITT analysis. It is true that higher probe intensity tends to flatten the phase of HHG [30], and the calculation of the pulse duration from the deduced phases can be underestimated using the second-order perturbation theory. However, it almost has no effect on qualitatively determining trajectory groups based on the sign of slope of the line connecting the sideband oscillation maxima. To confirm this, we also took data with a much lower probe intensity and found that the same sideband pattern was produced, although with slightly worse counting statistics. We further investigated this point using a strong field approximation (SFA) calculation (described below) and found that the sideband pattern changes little with IR probe intensity below 10^{12} W cm^{-2}, the intensity range used in this experiment.

4. Theoretical comparison

4.1. Single-atom response

We first investigate to what extent these results can be understood on the basis of the generation of harmonics from a single atom, without taking into account propagation effects in the gas medium. We begin with a brief summary of the semi-classical picture which identifies the major physical effects expected. In this picture, the ionized electron is tunnel-ionized at the initial time t_e. When the electric field reverses its direction, electrons can be pulled back and recollide with the ion core at the final time t_f, which indicates the emission time of HHG. The time pair (t_e, t_f) defines an electronic trajectory. HHG below the cutoff is attributed mainly to these two trajectory groups, short (with $\tau = t_f - t_e$ near a half optical cycle) and long (with τ near a full optical cycle) [24]. The phase, or the classical action of the electron trajectory which also approximately corresponds to the phase of the emitted harmonic, can be approximately expressed as $\phi_j(t) \approx -U_p\tau_j \approx -\alpha_j I(t)$ [15], where U_p is the pondermotive energy of the driving laser and τ_j is the electron excursion time for the jth trajectory. The constant α_j is roughly proportional to τ_j and $I(t)$, the time-dependent laser intensity. Therefore, the phase is proportional to the laser intensity. Since the long trajectory has a longer excursion time than that of the short trajectory, the magnitude of α_j is much larger for this case and the phase is more sensitive to the laser intensity than is that for the short trajectory [31]. The variation of intensity during the finite pulse duration leads to a corresponding time variation of the phase, and the time derivative of this appears as a frequency shift in the HHG spectrum. The leading-edge portion of the driving field corresponding to an increasing intensity with time will drive a blue shift, while the trailing-edge portion of the driving field will drive a red shift with a decrease of the intensity. The shift is much larger for the long trajectory than for the short one and thus should shift the frequencies for these two trajectories differently and lead to a spectral splitting for each harmonic. If HHG from both short and long trajectories are present and both were emitted only on the rising edge of the pulse, one would expect a large blue shift for the long trajectory and a small blue shift for the short trajectory. Similarly, the expected chirp of the HHG is expected to be different for the short and long trajectories. For short trajectories, the emission time increases with harmonic number, while for long trajectories, it decreases. As discussed in [24], this implies that in a RABBITT scan, a line drawn through the maxima of the sidebands will have a small positive slope (positive chirp), while the corresponding slope for long trajectories will be negative (negative chirp).

In order to evaluate this single-atom expectation quantitatively, we performed a quantum mechanical calculation of the HHG spectrum in a slightly modified version of the SFA. Using the Lewenstein model [32], the time-dependent dipole moment of an atom in a strong field is given as

$$D(t) = \mathrm{i}\int_0^\infty \mathrm{d}\tau \left(\frac{\pi}{\varepsilon + \mathrm{i}\tau/2}\right)^{3/2} \mathrm{d}^*[P_s(t,\tau) - A(t)]a^*(t) \times \exp(-\mathrm{i}S(P_s,t,\tau)) \times E(t-\tau)\cdot \mathrm{d}[P_s(t,\tau) - A(t-\tau)] \times a(t-\tau) + \mathrm{c.c.}, \quad (1)$$

where $d(p)$ is the transition dipole matrix element between the ground state and a continuum state with momentum p. $E(t)$ and $A(t)$ represent the electric field of the laser pulse and the associated vector potential, respectively, and ε is a positive regularization constant. P_S and $S(P,t,\tau)$ are the canonical momentum and quasi-classical action of the continuum electron, respectively. Ground-state depletion is included by introducing the ground-state amplitude $a(t) = \exp\left[-\frac{1}{2}\int_{-\infty}^{t} w(t')\,\mathrm{d}t'\right]$ [44], where $w(t)$ is the ionization rate calculated with the ADK model [33]. We denote the Fourier transform of $D(t)$ as the induced dipole $D(\omega)$, and the HHG intensity is proportional to $\omega^4\,|D(\omega)|^2$, the momentum of the free election p and the angular frequency of the harmonic photon ω is related by the energy conservation law: $\hbar\omega = p^2/2 + I_p$.

In the SFA model, the transition dipole element $d(p)$ is calculated assuming that the unbound electron is a free electron in the strong laser field. An improvement on this model, which incorporates the interaction of this electron with the residual ion, can be obtained using the 'quantitative rescattering' (QRS) model [34–36]. In this model, the induced dipole moment $D(\omega)$ can be written as the product of a returning electron wave packet $W(\omega)$ and the photo-emission transition dipole $d_e(\omega)$ of the atom from the stationary scattering calculation: $D(\omega) = W(\omega)d_e(\omega)$. The electron wave packet $W(\omega)$ is a property of the laser only and can be deduced by dividing the SFA expression in equation (1) by $d(p)$. The transition dipole $d_e(p)$ is then calculated using 'exact' numerical wavefunctions for the bound and continuum states within the single active electron approximation. The resulting expression for the induced dipole $D(\omega)$, which becomes the result from equation (1) multiplied by the ratio $d_e(\omega)/d(p)$, was used to calculate the HHG spectrum.

Figure 5(a) shows the depletion factor $a(t)$ and figure 5(b) shows the HHG spectrum of argon calculated using the QRS model. In the calculation, the excursion time of the electron is limited to one optical cycle to eliminate the contribution from high-order recollision processes. This assumption is reasonable and emphasizes the major physical effect due to the

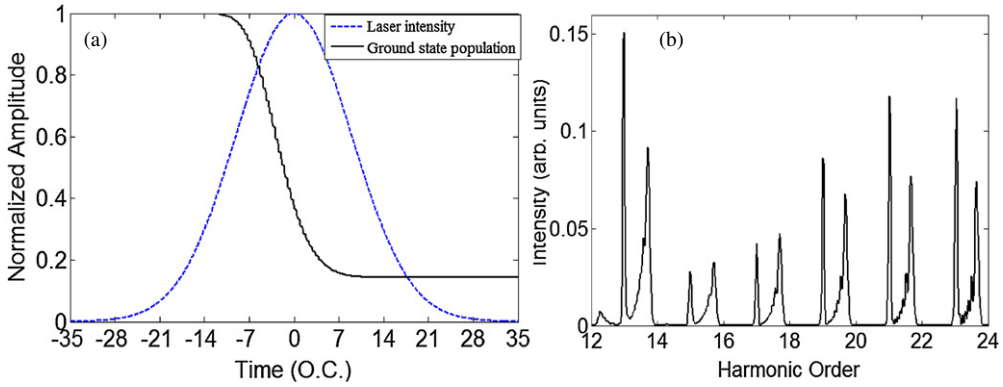

Figure 5. (a) The normalized laser intensity profile (blue dashed line) and the time-dependent ground-state population (black solid line) of argon. (b) The calculated HHG spectrum of argon under the single-atom response. The driving field is 60 fs with peak intensity of 3×10^{14} W cm^{-2}.

fact that high-order processes have more rapid phase variation because of the longer excursion time, and thus will die out quickly in the medium. The 60 fs long pulse has an intensity close to the saturation intensity of argon ($\sim 2 \times 10^{14}$ W cm^{-2}). In the model, the ground state is dramatically depleted, and harmonic generation ceases before the arrival of the peak of the pulse. Therefore, only blue shifts occur in the spectrum and short and long trajectories are separable in the frequency domain, with the higher frequency corresponding to the long trajectories.

Next we need to calculate the expected RABBITT spectrum. In the SFA, the IR-assisted EUV photo-ionization process can be simulated analytically [25]; the transition amplitude to the final continuum state $|v\rangle$ is given by

$$y(v,\tau) = -\mathrm{i}\int_{-\infty}^{+\infty} \mathrm{d}t\, \mathrm{e}^{\mathrm{i}\phi(t)} d_{p(t)} E_X(t-\tau)\, \mathrm{e}^{\mathrm{i}(W+I_P)t},$$
$$\phi(t) = -\int_{t}^{+\infty} \mathrm{d}t'[v \cdot A(t') + A^2(t')/2], \qquad (2)$$

where v is the momentum of the final continuum state $|v\rangle$. E_X(t) is the electric field of the EUV pulse, $A(t)$ is the vector potential of the IR field and d_P, W and I_P stand for the transition dipole moment, final kinetic energy of the electron and ionization potential of the target, respectively.

The right-hand panel of figure 6 shows the calculated RABBITT density plot of photoelectron yield versus EUV/IR delay. The spectrum of figure 5 is shown in the left-hand panel for reference. The calculated RABBITT spectrum shows clearly that the red and blue sidebands have very different phase behaviour. A line drawn through the maxima of the red sidebands shows a small positive slope, while that through the blue sidebands show a negative slope. These results are in agreement with the expectations of the semi-classical model, and allow us to assign the red sidebands to short trajectories and the blue sidebands to long trajectories. However, this correlation between slope and shift is exactly the opposite of that observed in the experiment, which seems to show that the blue sideband corresponds to the short trajectories. It is clear that the simple single-atom explanation fails to explain the data.

Note that the pulse duration and peak intensity that we used in the single-atom response are different from the

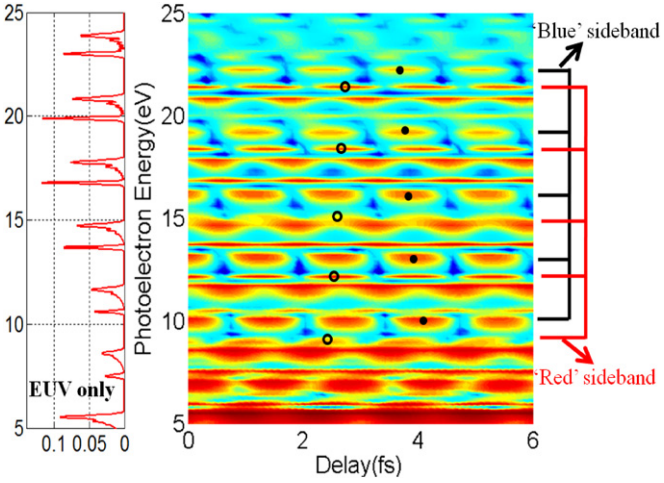

Figure 6. Left: the calculated photoelectron spectrum of argon when only EUV is present. Right: calculated EUV–IR cross-correlated traces. The HHG spectrum (figure 5(b)) used in the calculation is based on the single-atom response.

estimated experimental values. In the real experiment, the strong ionization of the medium by the laser will produce a considerable level of plasma. The dispersion of the plasma will tend to stretch the laser pulse and therefore reduce the peak intensity of the focused laser beam. Thus, it is reasonable to use a slightly longer pulse duration and lower peak intensity in the calculations to compare with the real experimental data.

4.2. Macroscopic effect

The disagreement between the single-atom response model and the experimental results shows the necessity of including propagation effects in the gas medium. These effects include three aspects in our case. The first is the phase matching coming from the phase velocity difference between the fundamental driving field and HHG field in the medium. The second is the plasma effect: because the laser intensity in our experiment is well above the saturation intensity of the gas, the plasma level could be appreciable. The nonlinearity of the plasma can induce distortion of the driving field in the time domain, which will eventually affect the HHG process. The third aspect is the absorption of the EUV in the gas medium.

The significant influence of the macroscopic effects for a long gas cell has been revealed by Ruchon *et al* [37]. All of these aspects can be taken into account by solving the coupled Maxwell equations in three dimensions. The details of the calculation can be found elsewhere [38–42]. We recall only the main equations here. The propagation of the fundamental field in an ionizing medium is described by

$$\nabla^2 E_1(r,z,t) - \frac{1}{c^2}\frac{\partial^2 E_1(r,z,t)}{\partial t^2} = \frac{\omega_0^2}{c^2}\left(1-\eta_{\text{eff}}^2\right)E_1(r,z,t), \quad (3)$$

where E_1 is the transverse electric field. The effective refractive index is

$$\eta_{\text{eff}}(r,z,r) = \eta_0(r,z,t) + \eta_2 I(r,z,t) - \frac{\omega_p^2(r,z,t)}{2\omega_0^2}. \quad (4)$$

The first two terms account for refraction, absorption and optical Kerr nonlinearity, and the third term describes the plasma effects with plasma frequency,

$$\omega_p = [e^2 n_e(t)/(\varepsilon_0 m_e)]^{1/2}, \quad (5)$$

where m_e and e are the mass and charge of an electron, respectively, and $n_e(t)$ is the density of free electrons. In the meanwhile, the propagation of the harmonic field is described by

$$\nabla^2 E_h(r,z,t) - \frac{1}{c^2}\frac{\partial^2 E_h(r,z,t)}{\partial t^2} = \mu_0 \frac{\partial^2 P(r,z,t)}{\partial t^2}. \quad (6)$$

The polarization $P(r, z, t)$ can be separated into linear and nonlinear components. The former one includes both linear dispersion and absorption effects of the HHG, and the latter one includes the so-called single-atom response and the remaining neutral atomic density. The single-atom response is calculated using the QRS theory [33–35]. Both equations (3) and (6) are solved by using the Crank–Nicholson routine in the frequency domain.

In the calculation [41], the on-axis propagation distance is 1.2 cm to mimic a semi-infinite gas cell. The real gas cell is 30 cm long and is much longer than the simulation length 1.2 cm. However, the laser does not see most of the gas cell in its optical path because only the very small focusing volume is the place where the laser distortion and HHG will take place. We used the region between the gas cell exit and 1.2 cm before the exit for the simulation. This is reasonable because outside this region, no appreciable flux will contribute due to the low laser intensity. According to the experimental conditions, the laser peak intensity, pulse duration and beam-waist in vacuum are 6×10^{14} W cm^{-2}, 50 fs and 25 μm, respectively. The focal position of the laser beam is set to be where the centre of the filamentation occurs. This position is approximately where the experimental focus is set for case III. However, this is not exact, since the laser beam in the medium can be self-focused and therefore the filamentation does not reflect the exact location of the focal point of the laser beam. The calculation is performed by integrating the differential equations from the very beginning to the end of the gas cell. At the exit of the gas cell, we will get the near-field EUV spectrum. In the experiment, the EUV will propagate in vacuum for 1 m before going through a 2 mm diameter hole mirror to combine with the IR probe beam. Thus, we perform a Hankel transformation on the calculated field to get the far-field distribution, and then an on-axis spatial filter is applied to select the HHG spectrum with a divergence less than 1 mrad to compare with the experimental data. Figure 7 shows the calculated far-field on-axis EUV spectrum. The splitting feature in the spectrum is well reproduced, similar to the single-atom response calculation. The IR-assisted photoionization spectrum was then calculated to extract the phase information of the calculated EUV spectrum (see figure 8). We can see that after including the propagation effect, the calculation shows that the blue sideband has the small positive slope, while the red sideband shows a negative slope, in agreement with the experimental data and exactly opposite to the single-atom response result. It is clear that taking propagation effects into account is essential to explain the phase behaviour of the observed spectral splitting.

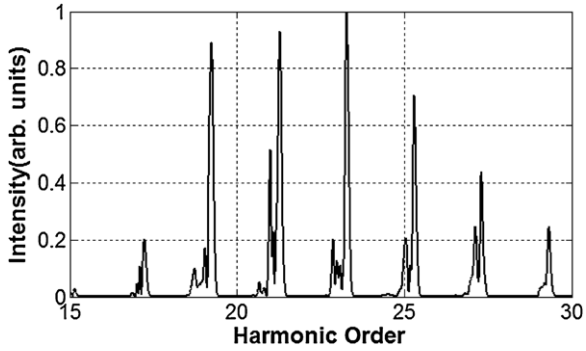

Figure 7. Calculated HHG spectrum at the far-field with divergence less than 1 mrad, the driving field is 50 fs with a peak intensity of 6×10^{14} W cm^{-2} and the focal point is in the middle of the 1.2 cm gas cell in vacuum.

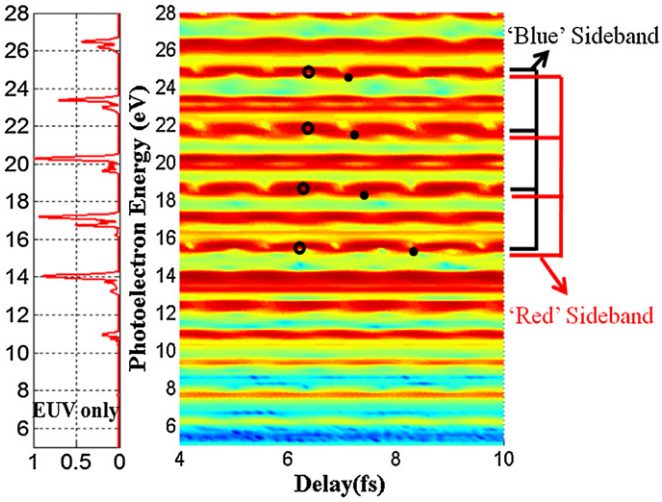

Figure 8. Left: the calculated photoelectron spectrum of argon when only EUV is present. Right: calculated EUV–IR cross-correlated traces. The HHG spectrum used in the calculation has included the propagation effect (see figure 7).

5. Discussion

The additional phase information available to us from the RABBITT scans presents strong evidence that the blue

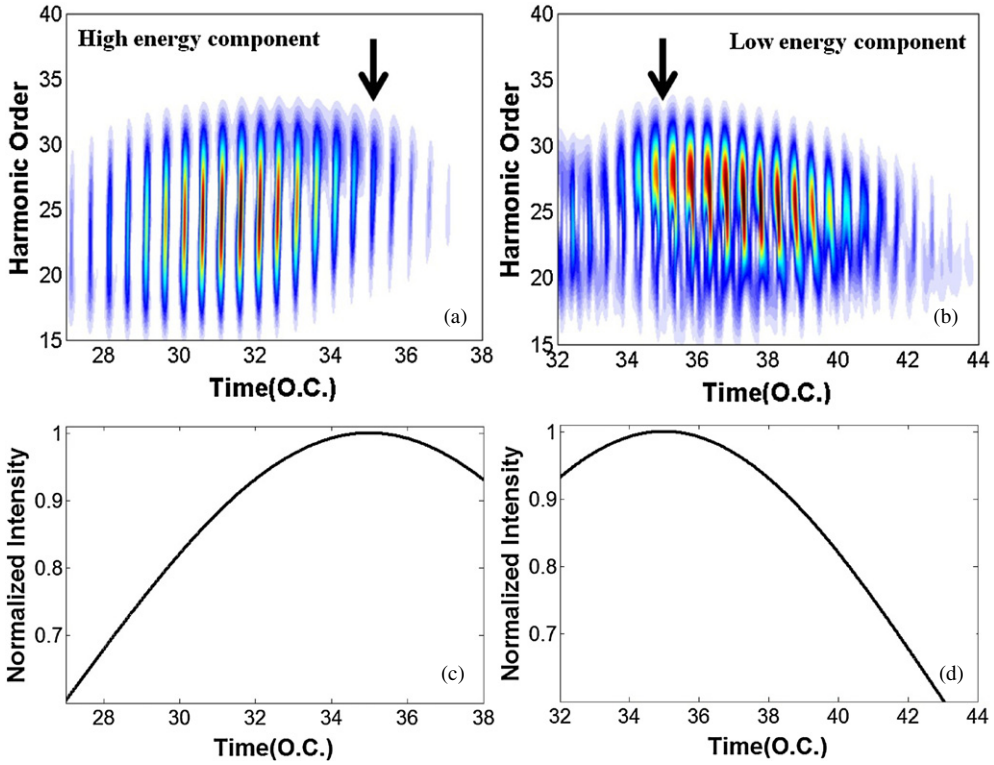

Figure 9. Time–frequency analysis of the HHG signal gated on the lower energy component (a) and the higher energy component (b) of the spectrum in figure 6. The black arrows indicate the location of the peak of the driving field. (c), (d) The normalized intensity profile of the laser in vacuum.

sideband in the split spectrum is due mainly to the short trajectories, not the long trajectories as might be expected on the basis of a single-atom response treatment. The full calculation including macroscopic effects is in agreement with the data. We now attempt to use this calculation to find why the short trajectory corresponds to the higher frequency component instead of the lower frequency component. While both absorption and plasma effects enter into the propagation calculation, the absorption of the gas medium typically only modifies the amplitude of the spectrum and has no contribution to the phase behaviour of the HHG. The phase matching issue is related to the coherent summation of XUV photons generated at different locations. It depends on the energy and space-dependent efficiency of harmonic generation, which is likely to be the major factor governing both the spectral splitting and the phase evolution of the HHG.

In order to probe more deeply the origin of the two harmonic side-peaks, an appropriate spectral gate was applied to select only one component of the double-peak harmonic signal. Then the time–frequency analysis was performed on the gated signal such that both frequency and timing information can be revealed simultaneously in a single spectrogram. Figure 9 shows the calculated spectrograms corresponding to different sub-peaks in the EUV spectrum of figure 7. The 'blue' or higher energy component for each harmonic order, which shows a reasonable positive chirp (lower frequency photons lead higher frequency photons), is generated at the leading edge close to the peak of the laser intensity profile. This indicates a clean short-trajectory group experiencing a small blue shift. On the other hand, the 'red' or lower energy component for each harmonic order is generated at the trailing edge of the laser pulse and therefore will experience a red shift in the frequency domain. It should be noted that in the experimental (figure 4) and simulated results (figure 8), the chirp of the sideband from the low-energy group is much larger than the expected one from the long-trajectory group alone. This is caused by the mixture of a weak short-trajectory signal with the long-trajectory group. The interference of the two groups will change the phase behaviour dramatically [43]. However, the long-trajectory behaviour is still dominating.

Why does the long trajectory favour the trailing edge of the laser pulse? One contributing factor comes from the evolution of the fundamental driving field. At a laser intensity close to or beyond the saturation intensity, free electrons can distort the fundamental field by introducing a nonlinear term into Maxwell's equations, which leads to a positive chirp in the carrier of the laser field after propagating for a certain distance. Based on the quantum mechanical theory under the SFA, the phase $\Phi(t)$ associated with each quantum trajectory or path is related to the intensity I and angular frequency ω of the driving field by approximately $\Phi(t) \propto \tau U_p \propto I\alpha/\omega^3$, where τ is the excursion time of the electronic trajectory. The larger the carrier frequency ω, the weaker the intensity dependence of the phase. Therefore, if the driving field is positively chirped (or the carrier frequency is increasing with time), high-order harmonics generated at the leading edge will experience a larger divergence than do those generated from the trailing edge of the laser field. Therefore, radiation from the long trajectory which is discriminated against by its larger angular divergence and small angular acceptance of the

experiment tends to escape this discrimination somewhat when it is generated on the trailing edge of the driving field. The short-trajectory radiation, which is characterized by a smaller angular divergence, has no need to await the higher driving frequency and can be generated efficiently on the leading edge of the driving field. Although the plasma-induced chirp on the fundamental field gives qualitative explanation, we do believe that this could be a much more complicated process including the plasma-induced dispersion, plasma-induced nonlinearity and the phase matching between the fundamental and HHG fields. Further studies are needed to fully understand the underlying mechanism.

6. Conclusion

The spectral splitting of HHG from a semi-infinite gas cell has been investigated experimentally. An EUV–IR cross-correlation (RABBITT) experiment has been carried out to characterize the phase behaviour (or to identify the quantum path) associated with each component of the split HHG. The result indicates that the high (low) energy component of each harmonic order is identified as a short (long) trajectory, which is counterintuitive and different from what the single-atom model predicts. By numerically solving the coupled Maxwell equations, the macroscopic effect of propagation through the medium is considered and a result is obtained in good agreement with the experiment. This agreement shows that a correct treatment of propagation effects such as the divergence of quantum paths of the HHG and the evolution of the fundamental field in the plasma is essential for a full understanding of the spectral splitting. Further investigations, including the use of pulse-shaping techniques and pulses with variable wavelengths, are among the potential applications of this interesting phenomenon.

Acknowledgments

This work was supported by Chemical Sciences, Geosciences and Biosciences Division, Office of Basic Energy Sciences, Office of Science, US Department of Energy; WC was supported by the National Science Foundation under grant no CHE-0822646. GL was supported by the US Army Research Office under grant no W911NF-07-1-0475.

References

[1] Hentschel M *et al* 2001 *Nature* **414** 509
[2] Paul P M *et al* 2001 *Science* **292** 1689
[3] Sansone G *et al* 2006 *Science* **314** 443
[4] Spielmann C *et al* 1997 *Science* **278** 661
[5] Chang Z *et al* 1997 *Phys. Rev. Lett.* **79** 2967
[6] Itatani J *et al* 2004 *Nature* **432** 867
[7] Li W *et al* 2008 *Science* **322** 1207
[8] Corkum P B 1993 *Phys. Rev. Lett.* **71** 1994
Krause J L, Schafer K J and Kulander K C 1992 *Phys. Rev. Lett.* **68** 3535
[9] Salières P *et al* 2001 *Science* **292** 902
[10] Lewenstein M, Salières P and L'Huillier A 1995 *Phys. Rev.* A **52** 4747
[11] López-Martens R *et al* 2005 *Phys. Rev. Lett.* **94** 033001
[12] Schafer K J *et al* 2004 *Phys. Rev. Lett.* **92** 023003
[13] Cao W *et al* 2007 *J. Phys. B: At. Mol. Opt. Phys.* **40** 869
[14] Brugnera L *et al* 2011 *Phys. Rev. Lett.* **107** 153902
[15] Zair A *et al* 2008 *Phys. Rev. Lett.* **100** 143902
[16] Schiessl K *et al* 2007 *Phys. Rev. Lett.* **99** 253903
[17] Wang Y, Liu Y, Yang X and Xu Z 2000 *Phys. Rev.* A **62** 063806
[18] Zhong F *et al* 2002 *Phys. Rev.* A **65** 033808
[19] Brunetti E, Issac R and Jaroszynski D A 2008 *Phys. Rev.* A **77** 023422
[20] Xu H, Xiong H, Zeng Z, Fu Y, Yao J, Li R, Cheng Y and Xu Z 2008 *Phys. Rev.* A **78** 033841
[21] He X *et al* 2009 *Phys. Rev.* A **79** 063829
[22] Véniard V, Taïeb R and Maquet A 1996 *Phys. Rev.* A **54** 721
[23] Paul P M, Toma E S, Breger P, Mullot G, Auge F, Balcou P, Muller H G and Agostini P 2001 *Science* **269** 1689
[24] Mairesse Y *et al* 2003 *Science* **302** 1540
[25] Mairesse Y and Quéré F 2005 *Phys. Rev.* A **71** 011401
[26] Steingrube D S *et al* 2009 *Phys. Rev.* A **80** 043819
[27] Ulrich J *et al* 1997 *J. Phys. B: At. Mol. Opt. Phys.* **30** 2917
[28] Dörner R *et al* 2000 *Phys. Rep.* **330** 95
[29] Antoine P, L' Huillier A and Lewenstein M 1996 *Phys. Rev. Lett.* **77** 1234
[30] Swoboda M *et al* 2009 *Laser Phys.* **19** 1591
[31] Gaarde M B *et al* 1999 *Phys. Rev.* A **59** 1367
[32] Lewenstein M *et al* 1994 *Phys. Rev.* A **49** 2117
[33] Ammesov M V, Delone N B and Krainov V P 1986 *Zh. Eksp. Teor. Fiz.* **64** 1191
[33a] Tong X M and Lin C D 2005 *J. Phys. B: At. Mol. Opt. Phys.* **38** 2593
[34] Lin C D, Le A T, Chen Z, Morishita T and Lucchese R R 2010 *J. Phys. B: At. Mol. Opt. Phys.* **43** 122001
[35] Morishita T, Le A T, Chen Z and Lin C D 2008 *Phys. Rev. Lett.* **100** 013903
[36] Le A T, Lucchese R R, Tonzani S, Morishita T and Lin C D 2009 *Phys. Rev.* A **80** 013401
[37] Ruchon T *et al* 2008 *New J. Phys.* **10** 025027
[38] Priori E *et al* 2000 *Phys. Rev.* A **61** 063801
[39] Gaarde M B, Tate J L and Schafer K J 2008 *J. Phys. B: At. Mol. Opt. Phys.* **41** 132001
[40] Tosa V, Kim H T, Kim I J and Nam C H 2005 *Phys. Rev.* A **71** 063807
[41] Jin C, Le A T and Lin C D 2011 *Phys. Rev.* A **83** 023411
[42] Jin C *et al* 2011 *J. Phys. B: At. Mol. Opt. Phys.* **44** 095601
[43] Kruse J E *et al* 2010 *Phys. Rev.* A **82** 021402
[44] Jin C, Le A T and Lin C D 2009 *Phys. Rev.* A **79** 053413